SCIENCE CHINA
Information Sciences

• RESEARCH PAPER •

February 2018, Vol. 61 022301:1–022301:14
doi: 10.1007/s11432-016-9032-6

Equivalent system model for the calibration of polarimetric SAR under Faraday rotation conditions

Jingjing ZHANG[1,2] & Wen HONG[1,2*]

[1]*Science and Technology on Microwave Imaging Laboratory, Institute of Electronics, Chinese Academy of Sciences, Beijing* 100190*, China;*
[2]*University of Chinese Academy of Sciences, Beijing* 100049*, China*

Received 5 December 2016/Revised 16 January 2017/Accepted 16 February 2017/Published online 25 August 2017

Abstract An equivalent system model (ESM) that can be used to calibrate a SAR system affected by both the effect of system errors and the Faraday rotation (FR) is proposed. This ESM contains only system-distortion-like parameters but includes a distortion matrix (DM) that is identical to the original, which contains the effects of both the system errors and the Faraday rotation angle (FRA). With this model, the conventional distributed-target-based (DT-based) algorithms which have not taken FR effect into account are readily applicable. The conditions on FRA for the successful application of DT-based algorithms are studied, and the results suggest that reliable estimates can be obtained for a well-designed system whose true system crosstalk level is lower than −20 dB provided that the mean FRA at the calibration site is within ±15° and that the FRA can be suitably modeled as Gaussian. Thus, the requirements on the crosstalk level or the FRA that are commonly employed in other calibration methods designed for data affected by FR are relaxed.

Keywords calibration, Faraday rotation (FR), polarimetry, distibuted target (DT), synthetic aperture radar (SAR)

Citation Zhang J J, Hong W. Equivalent system model for the calibration of polarimetric SAR under Faraday rotation conditions. Sci China Inf Sci, 2018, 61(2): 022301, doi: 10.1007/s11432-016-9032-6

1 Introduction

Spaceborne polarimetric synthetic aperture radars (SARs) operating at long wavelengths (e.g., in the L-band and P-band) provide valuable data for several earth science applications [1–3]. However, observations made by such systems suffer from the effects of both polarimetric system distortions and Faraday rotation (FR). These effects must be removed for meaningful polarization information about a target to be extracted. To correct the errors induced by these effects, many techniques have been developed and can be roughly categorized into two groups. The algorithms in the first group treat the system distortions and the Faraday rotation angle (FRA) independently [4, 5] by assuming either that the crosstalk is negligible [4] or that the FRA can be ignored [5]. These assumptions, especially the former, are difficult to satisfy; therefore, the ranges of application of these algorithms are limited. In the second group, the distortion matrix (DM) induced by the effects of system distortions and FR together is estimated; examples of such algorithms include one that uses the polarimetric orientation angle (POA) in build-up areas [6] and one that uses covariance matrix matching estimation techniques (COMET) [7]. Although

* Corresponding author (email: whong@mail.ie.ac.cn)

these methods are locally valid, they fail to consider the spatial dependence of the system errors and FRA.

Practical methods of addressing the range dependence of distortions are based on the statistics of distributed targets (DTs) [8–15]. These DT-based methods were originally devised to address the FR-free case and had been successfully applied to calibrate several airborne SARs. However, only system distortions are considered in these methods, thereby precluding their direct application to data affected by FR.

Previous findings have shown that the FRA produces effects similar to those of system errors in uncalibrated data [4,16]. However, to date, no quantitative analysis has been performed. In this paper, we propose an equivalent system model (ESM) that can be used to quantify how the FRA affects system distortions. This ESM contains only system-distortion-like parameters but includes a DM that is identical to the original, which contains the effects of both the system errors and the FRA. Thus, when this ESM is used, existing DT-based methods are readily applicable.

This paper begins with an introduction to the distortion model, presented in Section 2. The ESM is developed in Section 3. The conditions on the FRA for the successful application of DT-based algorithms are studied in Section 4. Section 5 presents the calibration methods. Finally, the effectiveness of the approach is verified via Monte Carlo simulations in Section 6.

2 Distortion model

For a spaceborne polarimetric SAR operating at long wavelengths, the actual scattering matrix $\boldsymbol{S}$ is affected by the transmitting system $\boldsymbol{T}$, the receiving system $\boldsymbol{R}$, the one-way FR $\boldsymbol{F}$, and the noise $\boldsymbol{N}$. For each pixel in an SAR image, the measured scattering matrix $\boldsymbol{M}$ is related to $\boldsymbol{S}$ via [17,18]

$$\boldsymbol{M} = \boldsymbol{RFSFT} + \boldsymbol{N} \tag{1a}$$

or

$$\begin{bmatrix} M_{\rm HH} & M_{\rm HV} \\ M_{\rm VH} & M_{\rm VV} \end{bmatrix} = \begin{bmatrix} R_{\rm HH} & R_{\rm HV} \\ R_{\rm VH} & R_{\rm VV} \end{bmatrix} \begin{bmatrix} \cos\Omega & \sin\Omega \\ -\sin\Omega & \cos\Omega \end{bmatrix} \begin{bmatrix} S_{\rm HH} & S_{\rm HV} \\ S_{\rm VH} & S_{\rm VV} \end{bmatrix} \begin{bmatrix} \cos\Omega & \sin\Omega \\ -\sin\Omega & \cos\Omega \end{bmatrix} \begin{bmatrix} T_{\rm HH} & T_{\rm HV} \\ T_{\rm VH} & T_{\rm VV} \end{bmatrix} + \begin{bmatrix} N_{\rm HH} & N_{\rm HV} \\ N_{\rm VH} & N_{\rm VV} \end{bmatrix}. \tag{1b}$$

Here, Ω is the FRA. To rewrite (1) in vector form, we define the following system distortions in terms of the matrix elements $T_{\rm pq}$ and $R_{\rm pq}$ [4,12]:

$$\begin{aligned} Y = T_{\rm VV}R_{\rm VV}, \quad k = R_{\rm HH}/R_{\rm VV}, \quad \alpha = T_{\rm HH}R_{\rm VV}/T_{\rm VV}R_{\rm HH}, \\ u = R_{\rm VH}/R_{\rm HH}, \quad v = T_{\rm VH}/T_{\rm VV}, \quad w = R_{\rm HV}/R_{\rm VV}, \quad z = T_{\rm HV}/T_{\rm HH}, \end{aligned}$$

where Y is the overall gain, k is the co-pol imbalance, α is the cross-pol imbalance, and u, v, w, and z are the crosstalks. For notational convenience, we also introduce the following matrix symbols:

$$\boldsymbol{X}(u,v,w,z) = \begin{bmatrix} 1 & w & v & wv \\ u & 1 & uv & v \\ z & wz & 1 & w \\ uz & z & u & 1 \end{bmatrix}, \ \boldsymbol{A}(\alpha) = \begin{bmatrix} \alpha & 0 & 0 & 0 \\ 0 & \alpha & 0 & 0 \\ 0 & 0 & 1 & 0 \\ 0 & 0 & 0 & 1 \end{bmatrix}, \ \boldsymbol{K}(k) = \begin{bmatrix} k^2 & 0 & 0 & 0 \\ 0 & k & 0 & 0 \\ 0 & 0 & k & 0 \\ 0 & 0 & 0 & 1 \end{bmatrix},$$

$$\boldsymbol{\Omega}(\Omega) = \begin{bmatrix} 1 & \tan\Omega & -\tan\Omega & -\tan^2\Omega \\ -\tan\Omega & 1 & \tan^2\Omega & -\tan\Omega \\ \tan\Omega & \tan^2\Omega & 1 & \tan\Omega \\ -\tan^2\Omega & \tan\Omega & -\tan\Omega & 1 \end{bmatrix} \times \cos^2\Omega. \tag{2}$$

Then, Eq. (1) can be rewritten as

$$\underline{\boldsymbol{M}} = Y\boldsymbol{X}(u,v,w,z)\boldsymbol{A}(\alpha)\boldsymbol{K}(k)\boldsymbol{\Omega}(\Omega)\underline{\boldsymbol{S}} + \underline{\boldsymbol{N}}. \tag{3}$$

A line under a matrix symbol denotes the lexicographic column vectorization of the elements in the matrix. For example, $\underline{\boldsymbol{M}} = [M_{\mathrm{HH}}, M_{\mathrm{VH}}, M_{\mathrm{HV}}, M_{\mathrm{VV}}]^{\mathrm{T}}$. The vectors $\underline{\boldsymbol{S}}$ and $\underline{\boldsymbol{N}}$ are defined similarly.

3 Equivalent system model

The basic observable for a DT calibration site is the average covariance matrix computed from the distorted returns. Because the system distortions can be assumed to be invariant along the azimuth for a narrow-band SAR system, the averaging is typically performed along an azimuth line at constant range under FR-free conditions. For each range value, the average covariance matrix under FR-free conditions is

$$\boldsymbol{C} \triangleq \langle \underline{\boldsymbol{M}}\underline{\boldsymbol{M}}^{\dagger} \rangle\big|_{\Omega=0} = \boldsymbol{X}(u,v,w,z)\boldsymbol{A}(\alpha)\boldsymbol{K}(k)\langle \underline{\boldsymbol{S}}\underline{\boldsymbol{S}}^{\dagger} \rangle \boldsymbol{K}^{\dagger}(k)\boldsymbol{A}^{\dagger}(\alpha)\boldsymbol{X}^{\dagger}(u,v,w,z)|Y|^2, \tag{4}$$

where $\langle\cdot\rangle$ denotes the expectation and $\boldsymbol{\Sigma} \triangleq \langle \underline{\boldsymbol{S}}\underline{\boldsymbol{S}}^{\dagger} \rangle$ is the target covariance matrix. Nevertheless, in the presence of FR, the observed covariance matrix can be evaluated to be

$$\boldsymbol{C}' \triangleq \langle \underline{\boldsymbol{M}}\underline{\boldsymbol{M}}^{\dagger} \rangle\big|_{\Omega=\omega} = \boldsymbol{X}(u,v,w,z)\boldsymbol{A}(\alpha)\boldsymbol{K}(k)\langle \boldsymbol{\Omega}(\omega)\underline{\boldsymbol{S}}\underline{\boldsymbol{S}}^{\dagger}\boldsymbol{\Omega}^{\dagger}(\omega) \rangle \boldsymbol{K}^{\dagger}(k)\boldsymbol{A}^{\dagger}(\alpha)\boldsymbol{X}^{\dagger}(u,v,w,z)|Y|^2, \tag{5}$$

where ω denotes the FRA at the DT calibration site.

Typically, the FRA is spatially varying; therefore, we decompose the FRA at the range of interest as follows:

$$\omega = \overline{\omega} + \Delta\omega, \tag{6}$$

where $\overline{\omega}$ is the mean FRA at that range, which exhibits no azimuth dependence, and $\Delta\omega$ is the residual FRA, which represents the variation in the FRA along the azimuth. Using the identity $\boldsymbol{\Omega}(\omega_1+\omega_2) = \boldsymbol{\Omega}(\omega_1)\boldsymbol{\Omega}(\omega_2)$, we can show that

$$\langle \boldsymbol{\Omega}(\omega)\underline{\boldsymbol{S}}\underline{\boldsymbol{S}}^{\dagger}\boldsymbol{\Omega}^{\dagger}(\omega) \rangle = \boldsymbol{\Omega}(\overline{\omega})\langle \boldsymbol{\Omega}(\Delta\omega)\underline{\boldsymbol{S}}\underline{\boldsymbol{S}}^{\dagger}\boldsymbol{\Omega}^{\dagger}(\Delta\omega) \rangle \boldsymbol{\Omega}^{\dagger}(\overline{\omega}) = \boldsymbol{\Omega}(\overline{\omega})\boldsymbol{\Sigma}'\boldsymbol{\Omega}^{\dagger}(\overline{\omega}), \tag{7}$$

where $\boldsymbol{\Sigma}'$ is the target covariance matrix disturbed by the residual FRA. By substituting (7) into (5), we obtain

$$\boldsymbol{C}' = \boldsymbol{X}(u,v,w,z)\boldsymbol{A}(\alpha)\boldsymbol{K}(k)\boldsymbol{\Omega}(\overline{\omega})\boldsymbol{\Sigma}'\boldsymbol{\Omega}^{\dagger}(\overline{\omega})\boldsymbol{K}^{\dagger}(k)\boldsymbol{A}^{\dagger}(\alpha)\boldsymbol{X}^{\dagger}(u,v,w,z)|Y|^2. \tag{8}$$

Let us define the system-induced DM as

$$\boldsymbol{D} \triangleq Y\boldsymbol{X}(u,v,w,z)\boldsymbol{A}(\alpha)\boldsymbol{K}(k); \tag{9}$$

then, $\boldsymbol{D}' \triangleq \boldsymbol{D}\boldsymbol{\Omega}(\overline{\omega})$ defines the DM attributed to both the system errors and the mean FRA. We can then rewrite $\boldsymbol{D}'$ as (see Appendix A)

$$\boldsymbol{D}' = Y'\boldsymbol{X}(u',v',w',z')\boldsymbol{A}(\alpha')\boldsymbol{K}(k'), \tag{10}$$

where

$$\begin{aligned} Y' =& Y\frac{(1-ztk\alpha)(1+utk)}{1+t^2}, \quad k' = k\frac{1-wt/k}{1+utk}, \quad \alpha' = \alpha\frac{(1+utk)(1+vt/k\alpha)}{(1-ztk\alpha)(1-wt/k)}, \\ u' =& \frac{u-t/k}{1-wt/k}, \quad v' = \frac{v-tk\alpha}{1-ztk\alpha}, \quad w' = \frac{w+tk}{1+utk}, \quad z' = \frac{z+t/k\alpha}{1+vt/k\alpha} \end{aligned} \tag{11}$$

are referred to as the equivalent system distortions. In (11), $t = \tan\overline{\omega}$. This result indicates that the DM induced by the system errors and the mean FRA is identical to the DM in an ESM with only system-distortion-like parameters.

Using (10) in (8), we find that

$$\boldsymbol{C}' = \boldsymbol{X}(u',v',w',z')\boldsymbol{A}(\alpha')\boldsymbol{K}(k')\boldsymbol{\Sigma}'\boldsymbol{K}^{\dagger}(k')\boldsymbol{A}^{\dagger}(\alpha')\boldsymbol{X}^{\dagger}(u',v',w',z')|Y'|^2. \tag{12}$$

Comparing (12) with (4), we can see that the equivalent system distortions affect $\boldsymbol{\Sigma}'$ in the same manner as the system distortions affect $\boldsymbol{\Sigma}$. As a result, it seems possible to apply the existing DT-based algorithms [8–15], which were originally developed for the FR-free case, to data affected by FR using the ESM.

4 Conditions on the FRA

Successful application of existing DT-based algorithms requires the magnitudes of the crosstalks to be lower than a certain threshold $x_{\rm th}$ (between 0 and 1) and requires the target covariance matrix $\boldsymbol{\Sigma}$ to take a specific form. However, the mean FRA will modify the values of the equivalent crosstalks, and the residual-FRA-disturbed target covariance matrix $\boldsymbol{\Sigma}'$ may not take the required form. Thus, in this section, we investigate the conditions on the FRA for the equivalent crosstalks and $\boldsymbol{\Sigma}'$ to satisfy the aforementioned requirements.

4.1 Conditions on the mean FRA

In this subsection, we will study the conditions on the mean FRA for the equivalent crosstalks to be less than $x_{\rm th}$. First, we formalize the following definitions:

$$f \triangleq \max\big\{|f_1|, |f_2|, |1/f_1|, |1/f_2|\big\}, \tag{13}$$

$$x \triangleq \max\big\{|u|, |v|, |w|, |z|\big\}, \tag{14}$$

$$x' \triangleq \max\big\{|u'|, |v'|, |w'|, |z'|\big\}, \tag{15}$$

where x is the level of crosstalk in the system, f is the level of transceiver imbalance in the system, and x' is the equivalent crosstalk level in the ESM. In (13), $f_1 = R_{\rm HH}/R_{\rm VV} = k$ and $f_2 = T_{\rm HH}/T_{\rm VV} = k\alpha$ are the reception and transmission channel imbalances, respectively. For a well-designed polarimetric SAR system, it is reasonable to assume that x and f are within the ranges specified in Table 1.

The equivalent crosstalk terms are functions of the system distortions and the mean FRA; hence, x' is also a function of these quantities. Therefore, x' can be expressed as

$$x'(\boldsymbol{\theta}, \overline{\omega}) = \max\Big\{|u'(\boldsymbol{\theta}, \overline{\omega})|, |v'(\boldsymbol{\theta}, \overline{\omega})|, |w'(\boldsymbol{\theta}, \overline{\omega})|, |z'(\boldsymbol{\theta}, \overline{\omega})|\Big\}, \tag{16}$$

where the system distortion vector $\boldsymbol{\theta}$ is given by

$$\boldsymbol{\theta} \triangleq \big(|u|,\angle u,|v|,\angle v,|w|,\angle w,|z|,\angle z, |f_1|,\angle f_1,|f_2|,\angle f_2\big). \tag{17}$$

All distortion parameters are expressed in angle notation. For example, $|u|$ and $\angle u$ are the magnitude and phase, respectively, of u. It is straightforward to show that x' is a periodic function of $\overline{\omega}$ with a period equal to 180°, i.e., $x'(\boldsymbol{\theta}, \overline{\omega} + 180^\circ) = x'(\boldsymbol{\theta}, \overline{\omega})$. Thus, only the interval $[-90^\circ, +90^\circ)$ need be considered.

In Figure 1, we present how the crosstalk levels vary with the mean FRA for different configurations of polarimetric SAR systems. The dashed line corresponds to an ideal system with zero crosstalk and unit imbalances, and the solid line corresponds to an imperfect system with the following distortion parameters: $k = 1/\sqrt{2}$, $\alpha = 2\angle\ 30^\circ$, $u = 0.1\angle\ 60^\circ$, $v = 0.1\angle\ 90^\circ$, $w = 0.1\angle\ 120^\circ$, and $z = 0.1\angle\ 150^\circ$. It can be seen that x' is generally small when $\overline{\omega}$ is near 0°. Therefore, a site where (e.g., Amazon forest near the equator [5,19]) or when (e.g., a winter night [20]) the FRA is expected to be small is best suited for the determination of crosstalks, and a site with large (outside ±45°) or unpredictable FRAs should be avoided for calibration purposes. In the following discussion on the permissible values of the mean FRA, $\overline{\omega}$ is restricted to lie within ±45°.

Given the value of $\boldsymbol{\theta}$, the permissible values of the mean FRA for $x' \leqslant x_{\rm th}$ must belong to the following set:

$$\Omega = \big\{\, \overline{\omega} \,|\, x'(\boldsymbol{\theta}, \overline{\omega}) \leqslant x_{\rm th} \big\}. \tag{18}$$

Through examination of the curve of $x'(\boldsymbol{\theta}, \overline{\omega})$, Ω can be straightforwardly obtained. For example, let $x_{\rm th} = 0.5$; then, the permissible values of the mean FRA for the considered imperfect system can be found, from Figure 1, to be approximately,

$$\Omega \simeq [-16^\circ, 21^\circ]. \tag{19}$$

Knowledge of the allowed range of the mean FRA can guide us in selecting an appropriate DT calibration site. However, Ω is generally not known because the value of $\boldsymbol{\theta}$ is not known until we have performed

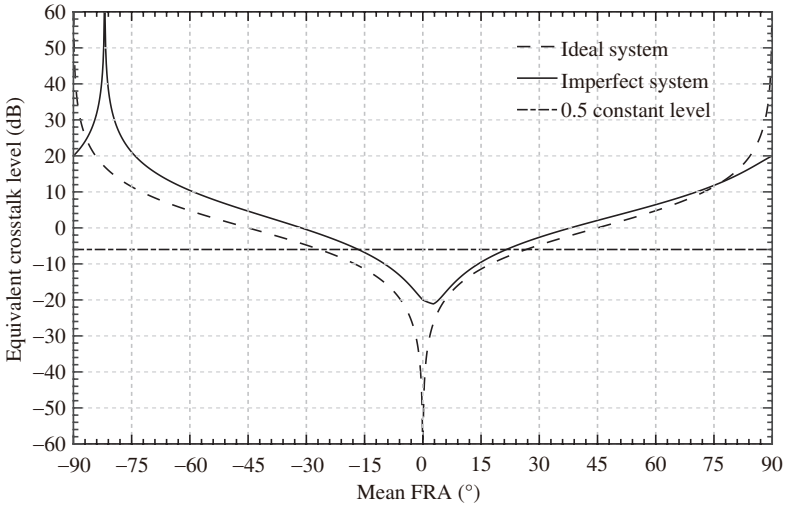

Figure 1 Equivalent crosstalk level versus mean FRA. The dashed line corresponds to an ideal system with zero crosstalk and unit imbalances. The solid line corresponds to an imperfect system with the following distortion parameters: $k = 1/\sqrt{2}$, $\alpha = 2\angle\ 30^\circ$, $u = 0.1\angle\ 60^\circ$, $v = 0.1\angle\ 90^\circ$, $w = 0.1\angle\ 120^\circ$, and $z = 0.1\angle\ 150^\circ$.

Table 1 Ranges of the true system distortions for a well-designed system

Parameter	Range
Crosstalk level (dB)	$[-50, -20]$
Crosstalk phase (°)	$(-180^\circ, +180^\circ]$
Transceiver imbalance level (dB)	$[0, 3]$
Transceiver phase imbalance (°)	$(-180^\circ, +180^\circ]$

the calibration using a suitable DT calibration site. To resolve this dilemma, we define the worst-case crosstalk level in the ESM as

$$\widetilde{x}'(\overline{\omega}) = \max_{\boldsymbol{\theta}} \left\{ x'(\boldsymbol{\theta}, \overline{\omega}) \right\}. \tag{20}$$

Then, the set

$$\Omega' \triangleq \left\{ \overline{\omega} \mid \widetilde{x}'(\overline{\omega}) \leqslant x_{\rm th} \right\}, \tag{21}$$

which is a subset of Ω, can be regarded as a conservative estimate of the allowed range of the mean FRA for a system whose distortion parameters are not known a priori.

Given the ranges for the components of $\boldsymbol{\theta}$ that are specified in Table 1, $\widetilde{x}'(\overline{\omega})$ can be evaluated to be (see Appendix B)

$$\widetilde{x}'(\overline{\omega}) = \max_{\boldsymbol{\theta}} \left\{ x'(\boldsymbol{\theta}, \overline{\omega}) \right\} = \frac{x + f|t|}{1 - xf|t|}. \tag{22}$$

Then, it is straightforward to show that

$$\Omega' = \left\{ \overline{\omega} \mid \overline{\omega} \in [-\Omega_0,\ \Omega_0] \right\}, \tag{23}$$

where $\Omega_0 = \tan^{-1}\left\{(x_{\rm th} - x)/(x_{\rm th}x + 1)f\right\}$. Table 2 lists the values of Ω' for several typical combinations of (f, x) when we set $x_{\rm th} = 0.5$. The results suggest that the ESM should only be used in the case of small FRAs because in the presence of a large FRA, the equivalent crosstalk level is guaranteed to exceed $x_{\rm th}$ even for an ideal system.

The allowed range of the mean FRA increases from $\pm 15^\circ$ to $\pm 26^\circ$ when the combination (f, x) changes from the worst case $(3\,\text{dB}, -20\,\text{dB})$ to the ideal case $(0\,\text{dB}, -\infty\,\text{dB})$. This increase is so small that it is not worth placing overly stringent restrictions on the design specifications for (f, x), and the minimum requirement, i.e., an (f, x) of better than $(3\,\text{dB}, -20\,\text{dB})$, is used throughout this paper. Thus, we assert that the mean FRA at the calibration site should be within $\pm 15^\circ$ to ensure that the crosstalk level is less than 0.5.

Table 2 Conservative estimates of the allowable ranges of the mean FRA for typical combinations of channel imbalance and crosstalk level

f (dB)	x (dB)	Ω'
3	-20	$[-15°, +15°]$
3	-30	$[-18°, +18°]$
3	-40	$[-19°, +19°]$
1	-20	$[-17°, +17°]$
1	-30	$[-20°, +20°]$
1	-40	$[-21°, +21°]$
0	$-\infty$	$[-26°, +26°]$

It is worth mentioning that the choice of $x_{\rm th}$ depends on the algorithm used and the desired calibration accuracy. However, to date, no study has been dedicated to determining the value of $x_{\rm th}$ for each algorithm; therefore, an arbitrary value of 0.5, which has previously been used in [14, 15], is adopted in this work.

4.2 Residual FRA

Based on the assumptions that

(i) the backscattering from a DT is reciprocal;

(ii) the DT under study displays azimuthal symmetry, the target covariance matrix under FR-free conditions satisfies

$$\boldsymbol{\Sigma} = \begin{bmatrix} \Sigma_{11} & 0 & 0 & \Sigma_{14} \\ 0 & \Sigma_{\times} & \Sigma_{\times} & 0 \\ 0 & \Sigma_{\times} & \Sigma_{\times} & 0 \\ \Sigma_{14}^{*} & 0 & 0 & \Sigma_{44} \end{bmatrix}, \tag{24}$$

where $\Sigma_{11} \triangleq \langle |S_{\rm HH}|^2 \rangle$, $\Sigma_{44} \triangleq \langle |S_{\rm VV}|^2 \rangle$, $\Sigma_{\times} \triangleq \langle |S_{\rm VH}|^2 \rangle$, and $\Sigma_{14} \triangleq \langle S_{\rm HH} S_{\rm VV}^{*} \rangle$.

To ensure that the form of the residual-FRA-disturbed target covariance matrix $\boldsymbol{\Sigma}'$ matches that of $\boldsymbol{\Sigma}$ (in the sense that several of the matrix elements are zero), we must also adopt the following two assumptions in addition to the two mentioned above:

(iii) The backscatter and $\Delta\omega$ (and, hence, functions of $\Delta\omega$) are independent.

(iv) The distribution of $\Delta\omega$ is Gaussian with zero mean and a standard deviation of σ_{ω}, i.e., $\Delta\omega \sim \mathcal{N}(0, \sigma_{\omega}^2)$.

Based on these four assumptions, it can be shown that $\boldsymbol{\Sigma}'$ takes the following form (see Appendix C):

$$\boldsymbol{\Sigma}' = \begin{bmatrix} \Sigma_{11}' & 0 & 0 & \Sigma_{14}' \\ 0 & \beta & \beta' & 0 \\ 0 & \beta' & \beta & 0 \\ \Sigma_{14}'^{*} & 0 & 0 & \Sigma_{44}' \end{bmatrix}, \tag{25}$$

where Σ_{14}' and its conjugate are complex quantities and the remainder are real quantities. Note that the difference between the forms of $\boldsymbol{\Sigma}$ and $\boldsymbol{\Sigma}'$ lies in the fact that $\beta \leqslant \beta'$. The equality holds only when the FRA is spatially constant. Thus, among existing DT-based algorithms [8–15], only the more general ones presented in [13–15], which allow $\beta \neq \beta'$, need be considered in the following.

Note that although we need only assume that $\Delta\omega$ has a symmetric distribution about zero for $\boldsymbol{\Sigma}'$ to take the above form (see Appendix C), we adopt the assumption that the distribution of the FRA is Gaussian based on the observations made in [21, 22].

In summary, the sufficient conditions for the successful application of the DT-based algorithms of [13–15] using the ESM are that the mean FRA should be within $\pm 15°$ and that the FRA can be suitably modeled as Gaussian.

5 Calibration method

For those scenes where the FRA satisfies the conditions discussed previously (hereafter they are referred to as "normal scenes"), $\boldsymbol{D'}$ can be obtained by direct application of DT-based algorithm. However, the FRA varies spatially and temporally, there might be places where the FRA does not satisfy the aforementioned conditions. In this section, we first review how to estimate $\boldsymbol{D'}$ for a normal scene using the conventional DT-based algorithm. Then, the calibration method for the other scenes which do not meet the conditions (hereafter they are referred to as "abnormal scenes") is devised.

5.1 Normal scene

For normal scene, we are able to determine the equivalent crosstalks and cross-pol imbalance using the DT-based algorithms presented in [13–15]. The equivalent crosstalk level may be large under FR condition, so we choose Zhang's algorithm [15] of these algorithms to derive the crosstalk terms because it has been shown to be able to address large crosstalks. Once the equivalent crosstalk terms and the cross-pol imbalance have been determined, the measurement equation in (3) can be corrected to

$$\underline{\boldsymbol{M}}' \simeq Y'\boldsymbol{K}(k')\boldsymbol{\Omega}(\omega-\overline{\omega})\underline{\boldsymbol{S}}. \tag{26}$$

Starting from (26) and using a trihedral reflector, we can determine k' and Y' by following the method presented in [4]. Up to this point, we have obtained the $\boldsymbol{D'}$ for a normal scene. Fully calibrated data can be obtained after estimation and correction of the FRA difference $\omega-\overline{\omega}$ using the circular-polarization-based method [23].

5.2 Abnormal scene

If the system is stable, then the measurement recorded for an abnormal scene, with an FRA designated by $\omega_\times$, can be expressed as

$$\begin{aligned}\underline{\boldsymbol{M}} &= Y\boldsymbol{X}(u,v,w,z)\boldsymbol{A}(\alpha)\boldsymbol{K}(k)\boldsymbol{\Omega}(\omega_\times)\underline{\boldsymbol{S}}+\underline{\boldsymbol{N}}\\ &= \boldsymbol{D'}\boldsymbol{\Omega}(\omega_\times-\overline{\omega})\underline{\boldsymbol{S}}+\underline{\boldsymbol{N}}.\end{aligned} \tag{27}$$

In the above equation, $\boldsymbol{D'}$ is the DM we have obtained at an arbitrary scene where the FRA meets the conditions in previous section and $\overline{\omega}$ is the average FRA at that scene. Hence, the removal of the system distortion is then performed using

$$\underline{\boldsymbol{M}}' = \boldsymbol{D'}^{-1}\underline{\boldsymbol{M}} \simeq \boldsymbol{\Omega}(\omega_\times-\overline{\omega})\underline{\boldsymbol{S}}. \tag{28}$$

After estimation and correction of $\omega_\times-\overline{\omega}$ with the circular-polarization-based method, fully calibration is done. It can be seen that, fully calibrated data can be easily obtained for a stable system. In this work, we only discuss the case of stable system. How to calibrate an unstable system is out of the scope of this paper, we defer the discussion in future work.

6 Experiments on simulated data

In this section, we use Monte Carlo simulations to evaluate the effectiveness of the proposed calibration method for determining the equivalent crosstalks and cross-pol imbalance.

6.1 Simulated data generation

For each set of user inputs (i.e., the crosstalk level x, the transceiver imbalance level f, the cross-pol signal-to-noise-ratio $\mathrm{SNR}_\times$, the mean FRA $\overline{\omega}$, and the standard deviation of the FRA σ_ω) in the ranges specified in Tables 1 and 3, the calibration data were generated as follows:

Table 3 Parameters used to generate the natural target data

Parameter		Unit	Value
Seed covariance matrix elements	$\Sigma_{11}, \Sigma_{\times}, \Sigma_{44}$	m^2	$1, 0.2, 1$
	$\dfrac{\Sigma_{14}}{\sqrt{\Sigma_{11}\Sigma_{44}}}$	–	$0.4\mathrm{e}^{\mathrm{j}10^\circ}$
Cross-pol SNR	$\Sigma_{\times}/\Sigma_{+}$	dB	$[0, 20]$
Number of looks	L	–	10^5
FRA at DT calibration site	$\omega \sim \mathcal{N}(\overline{\omega}, \sigma_\omega^2)$	$^\circ$	$\overline{\omega} \in [0^\circ, 15^\circ]$ $\sigma_\omega \in [0^\circ, 10^\circ]$

(1) Using the seed covariance matrix $\boldsymbol{C}$, whose non-zero elements are specified in Table 3, a total of L scattering vectors were simulated via

$$\underline{\boldsymbol{S}}_\ell = \boldsymbol{C}^{1/2}\boldsymbol{\nu}_\ell, \quad \ell = 1, 2, \ldots, L,$$

where $\boldsymbol{C}^{1/2}$ satisfies $\boldsymbol{C}^{1/2}(\boldsymbol{C}^{1/2})^\dagger = \boldsymbol{C}$ and $\boldsymbol{\nu}_\ell$ is a realization of a 4×1 complex Gaussian random vector that satisfies $\langle \boldsymbol{\nu}_\ell \rangle = \boldsymbol{0}$ and $\langle \boldsymbol{\nu}_\ell \boldsymbol{\nu}_\ell^\dagger \rangle = \boldsymbol{I}$.

(2) For the given values of $\overline{\omega}$ and σ_ω, L FRA samples $\{\omega_\ell\}$ were generated using a Gaussian random number generator.

(3) For the given values of x and f, the magnitudes of the crosstalk terms were set to x and the magnitudes of f_1 and f_2 were randomly selected between f^{-1} and f. Both the crosstalk and transceiver imbalance phases were assigned random values on the interval $(-180^\circ, +180^\circ]$. Subsequently, we set $k = f_1$ and $\alpha = f_2/f_1$. The absolute gain Y is irrelevant in the context of polarimetric calibration; therefore, we set $Y = 1$ in the simulation.

(4) For the given value of $\mathrm{SNR}_\times$, the noise power $\Sigma_+ = \Sigma_\times/\mathrm{SNR}_\times$ was determined. By assuming the noise power in each channel to be equal and the noise in different channels to be uncorrelated, the noise covariance matrix can be evaluated as $\Sigma_+\boldsymbol{I}$. Then, the noise vectors were simulated in a manner similar to the first step.

(5) By applying the system distortions and the FRA effect to $\underline{\boldsymbol{S}}_\ell$ and then adding the noise to the result, we obtained a total of L observed target vectors as follows:

$$\underline{\boldsymbol{M}}_\ell = Y\boldsymbol{X}(u, v, w, z)\boldsymbol{A}(\alpha)\boldsymbol{K}(k)\boldsymbol{\Omega}(\omega_\ell)\underline{\boldsymbol{S}}_\ell + \underline{\boldsymbol{N}}_\ell, \quad \ell = 1, 2, \ldots, L. \tag{29}$$

Finally, the natural target data were generated via $\boldsymbol{C}' = L^{-1}\sum_{\ell=1}^{L}\underline{\boldsymbol{M}}_\ell\underline{\boldsymbol{M}}_\ell^\dagger$.

6.2 Error metric

Because the actual values of the equivalent system distortions are known in advance, the quality of the estimation can be evaluated by comparing the estimates of the system distortions with the actual values using the maximum normalized error (MNE) [24]. The original definition of the MNE presented in [24] is modified here for the purpose of assessing the calibration performance. Suppose that the estimates of u', v', w', z', and α' are $\hat{u}'$, $\hat{v}'$, $\hat{w}'$, $\hat{z}'$, and $\hat{\alpha}'$, respectively; then, the MNE for crosstalk removal alone is defined as

$$\mathrm{MNE}_{\boldsymbol{X}} = \sqrt{\lambda_{\max}\big\{(\boldsymbol{E}_{\boldsymbol{X}} - \boldsymbol{I})^\dagger(\boldsymbol{E}_{\boldsymbol{X}} - \boldsymbol{I})\big\}}, \tag{30}$$

where $\boldsymbol{E}_{\boldsymbol{X}} = \boldsymbol{X}^{-1}(\hat{u}', \hat{v}', \hat{w}', \hat{z}')\boldsymbol{X}(u', v', w', z')$ and $\lambda_{\max}$ denotes the largest eigenvalue of the enclosed matrix $(\boldsymbol{E}_{\boldsymbol{X}} - \boldsymbol{I})^\dagger(\boldsymbol{E}_{\boldsymbol{X}} - \boldsymbol{I})$. Similarly, the MNE for crosstalk and cross-pol imbalance removal is defined as

$$\mathrm{MNE}_{\boldsymbol{XA}} = \sqrt{\lambda_{\max}\big\{(\boldsymbol{E}_{\boldsymbol{XA}} - \boldsymbol{I})^\dagger(\boldsymbol{E}_{\boldsymbol{XA}} - \boldsymbol{I})\big\}}, \tag{31}$$

where

$$\boldsymbol{E}_{\boldsymbol{XA}} = \boldsymbol{A}^{-1}(\hat{\alpha}')\boldsymbol{X}^{-1}(\hat{u}', \hat{v}', \hat{w}', \hat{z}')\boldsymbol{X}(u', v', w', z')\boldsymbol{A}(\alpha'). \tag{32}$$

Table 4 Calibration requirements for polarimetry and interferometry[1)]

Item	Value
Residual crosstalk level	< -35 dB
Channel amplitude imbalance	0.2 dB (soil moisture)
Channel phase imbalance	$2^\circ \sim 5^\circ$

1) Recommendations from CEOS CAL/VAL. 2004. http://earth.esa.int/workshops/ceos_sar_2004/recommendation_at_ceos_cal.html.

$\mathrm{MNE}_{\boldsymbol{X}}$ represents the worst-case error that can be induced by correcting for the crosstalk using these estimates, and $\mathrm{MNE}_{\boldsymbol{XA}}$ represents the worst-case error that can be caused by removing both the crosstalk and cross-pol imbalance using these estimates.

6.3 Performance assessment criteria

The requirements for a good calibration as recommended by the Committee on Earth Observation Satellites (CEOS) Calibration/Validation (CAL/VAL) Working Group are shown in Table 4. If the residual crosstalk level is below -35 dB, then the value of $\mathrm{MNE}_{\boldsymbol{X}}$ can be computed to be less than -28.9 dB. If the uncompensated cross-pol imbalance is within ± 0.2 dB in amplitude and $\pm 5^\circ$ in phase, under the condition that the residual crosstalk level is lower than -35 dB, then the value of $\mathrm{MNE}_{\boldsymbol{XA}}$ can be evaluated to be lower than -18.9 dB. Thus, in terms of $\mathrm{MNE}_{\boldsymbol{X}}$ and $\mathrm{MNE}_{\boldsymbol{XA}}$, the calibration requirements are equivalent to the criteria $\mathrm{MNE}_{\boldsymbol{X}} < -28.9$ dB and $\mathrm{MNE}_{\boldsymbol{XA}} < -18.9$ dB. In the following, each trial is claimed to be successful if $\mathrm{MNE}_{\boldsymbol{X}} < -28.9$ dB and $\mathrm{MNE}_{\boldsymbol{XA}} < -18.9$ dB.

6.4 Experimental results

The parameter estimation performance is highly sensitive to the cross-pol SNR. Therefore, the first experiment was devoted to finding the minimum requirement on the cross-pol SNR. The parameter estimation performance was tested at different levels of $\mathrm{SNR}_\times$ varying from 0 to 20 dB in steps of 1 dB. For each value of $\mathrm{SNR}_\times$, 10^4 Monte Carlo experiments were conducted with the crosstalk level, transceiver imbalance level, mean FRA, and standard deviation of the FRA fixed to $x = -20$ dB, $f = 3$ dB, $\overline{\omega} = 10^\circ$, and $\sigma_\omega = 1^\circ$, respectively. The empirical success rate for each $\mathrm{SNR}_\times$ value was calculated by averaging over these 10^4 Monte Carlo trials, and the results are presented in Figure 2. The success rate is observed to gradually increase with increasing cross-pol SNR and reaches 100% when $\mathrm{SNR}_\times$ is greater than 11 dB, which indicates that an $\mathrm{SNR}_\times$ of at least 11 dB is necessary for the calibration procedure to perform well. In the following experiments, the cross-pol SNR was fixed to 12 dB, one decibel above the minimum requirement.

In Section 4, we asserted that the sufficient condition on the mean FRA for the successful application of DT-based algorithms is that the mean FRA should be within $\pm 15^\circ$. To verify this assertion, for each value of $\overline{\omega}$ ranging from -15° to $+15^\circ$ in steps of 1°, 10^4 simulations were conducted with the following parameters held fixed: $x = -20$ dB, $f = 3$ dB, $\sigma_\omega = 1^\circ$, and $\mathrm{SNR}_\times = 12$ dB. Figure 3 presents the success rate versus the mean FRA, and the results show that the proposed method succeeded in almost all experiments, with only one failure in a total of 3.1×10^5 experiments, hence justifying the assertion.

The purpose of the 3rd test was to demonstrate the robustness of the proposed method with respect to fluctuations in the FRA. For each value of σ_ω ranging from 0° to 10° in steps of 1°, 10^4 Monte Carlo experiments were performed with the following parameters held fixed: $x = -20$ dB, $f = 3$ dB, $\overline{\omega} = 10^\circ$, and $\mathrm{SNR}_\times = 12$ dB. Figure 4 shows the success rate versus the standard deviation of the FRA. In a total of 1.1×10^5 independent experiments, the algorithm failed only three times, thereby yielding the conclusion that fluctuations in the FRA have little impact on the performance of the algorithm. The one failure in the 2nd test and the three failures in the 3rd test are all attributed to the cross-pol SNR because all experiments succeeded when we increased the cross-pol SNR to 20 dB.

Note that in the simulations presented above, the worst-case system distortions were used, i.e., $x = -20$ dB and $f = 3$ dB. Thus, provided that $\mathrm{SNR}_\times$ is at least 12 dB, the proposed method is confirmed

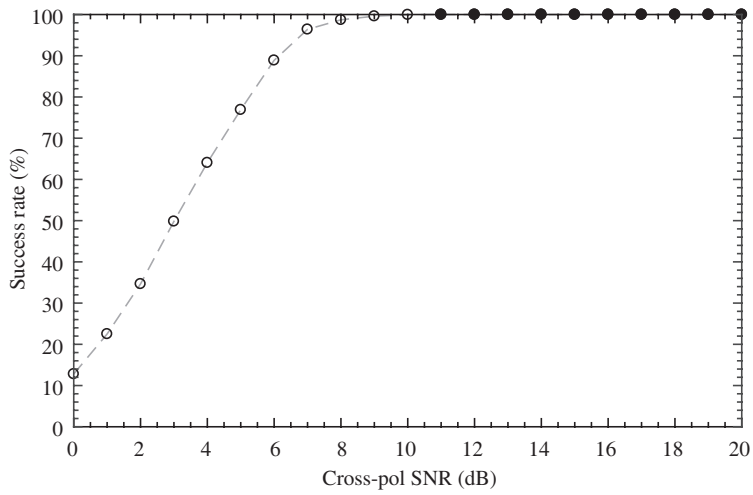

Figure 2 Success rate versus cross-pol SNR level obtained in 10^4 Monte Carlo trials with $\mathrm{SNR}_\times = 12\,\mathrm{dB}$, $\overline{\omega} = 10^\circ$, $x = -20\,\mathrm{dB}$, and $f = 3\,\mathrm{dB}$. A solid circle indicates that the corresponding value is exactly 100%.

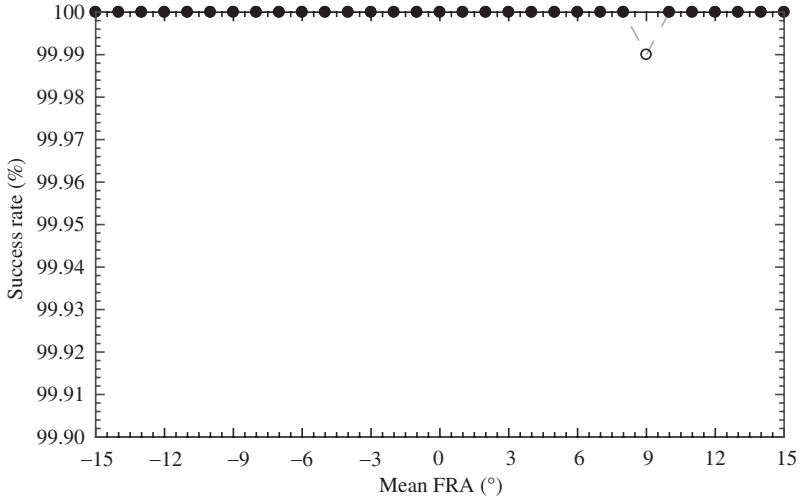

Figure 3 Success rate versus mean FRA obtained in 10^4 Monte Carlo trials with $\overline{\omega} = 10^\circ$, $\sigma_\omega = 1^\circ$, $x = -20\,\mathrm{dB}$, and $f = 3\,\mathrm{dB}$. A solid circle indicates that the corresponding value is exactly 100%.

to produce reliable estimates as long as the conditions on the FRA are satisfied.

The final test was devoted to a comparison of Freeman's method with the proposed one for inferring the cross-pol imbalance at different crosstalk levels. Note that Freeman's algorithm estimates α rather than α'; thus, to ensure comparable results, $\overline{\omega}$ was set to zero such that $\alpha' = \alpha$, $u' = u$, $v' = v$, $w' = w$, and $z' = z$. The test setup was as follows: the value of σ_ω was set to zero to represent the constant FR assumption that is implicitly adopted in [4], and f_1 was set to one for simplicity. For each value of x ranging from -50 to $-30\,\mathrm{dB}$ in steps of $1\,\mathrm{dB}$, 10^4 simulations were performed with $\mathrm{SNR}_\times = 12\,\mathrm{dB}$. Because the value of $\mathrm{MNE}_{\boldsymbol{X}}$ cannot be computed in Freeman's method, we report the average values of $\mathrm{MNE}_{\boldsymbol{XA}}$ rather than the success rates, as shown in Figure 5. Note that for Freeman's method, $\mathrm{MNE}_{\boldsymbol{XA}}$ is defined as

$$\mathrm{MNE}^{\mathrm{F}}_{\boldsymbol{XA}} = \sqrt{\lambda_{\max}\big\{(\boldsymbol{E}^{\mathrm{F}}_{\boldsymbol{XA}} - \boldsymbol{I})^\dagger(\boldsymbol{E}^{\mathrm{F}}_{\boldsymbol{XA}} - \boldsymbol{I})\big\}}, \tag{33}$$

where

$$\boldsymbol{E}^{\mathrm{F}}_{\boldsymbol{XA}} = \boldsymbol{A}^{-1}(\hat{\alpha}')\boldsymbol{X}(u', v', w', z')\boldsymbol{A}(\alpha'). \tag{34}$$

The average values of $\mathrm{MNE}_{\boldsymbol{XA}}$ for the proposed procedure are found to remain nearly constant regardless of the crosstalk level, whereas the average values of $\mathrm{MNE}^{\mathrm{F}}_{\boldsymbol{XA}}$ vary significantly with the crosstalk level

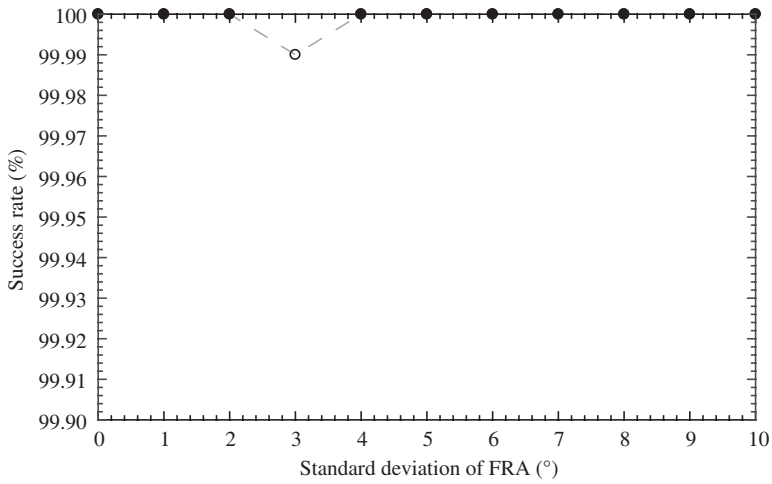

Figure 4 Success rate versus standard deviation of the FRA obtained in 10^4 Monte Carlo trials with $\mathrm{SNR}_{\times} = 12\,\mathrm{dB}$, $\sigma_\omega = 1^\circ$, $x = -20\,\mathrm{dB}$, and $f = 3\,\mathrm{dB}$. A solid circle indicates that the corresponding value is exactly 100%.

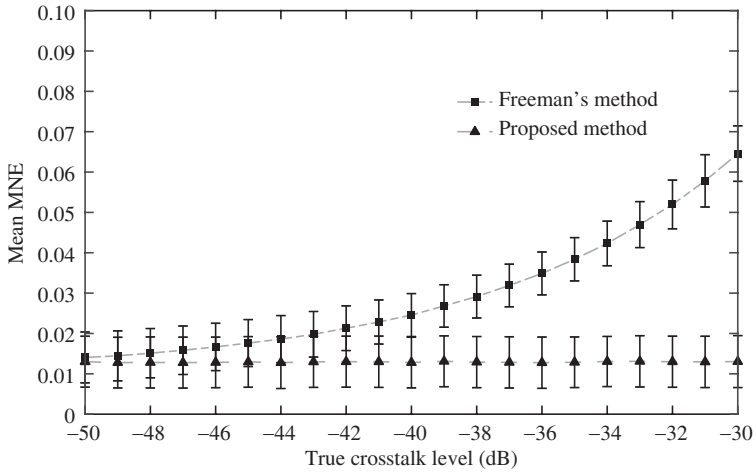

Figure 5 Mean value of $\mathrm{MNE}_{\boldsymbol{XA}}$ versus true crosstalk level obtained as the average from 10^4 Monte Carlo trials with $\mathrm{SNR}_{\times} = 12\,\mathrm{dB}$, $\overline{\omega} = 0^\circ$, $\sigma_\omega = 0^\circ$, $f = 3\,\mathrm{dB}$, and $f_1 = 1$. The length of each error bar corresponds to twice the standard deviation.

and are always larger. For the accuracy of Freeman's method to be comparable to that of the proposed one, the crosstalk level must be less than $-50\,\mathrm{dB}$.

7 Conclusion

A novel ESM that is suitable for the calibration of a polarimetric SAR affected by system distortions and the FR effect was developed. With this model, the crosstalks and cross-pol imbalance in the ESM can be estimated using DT-based algorithms. The conditions on the FRA for the successful application of DT-based algorithms were studied, and the findings suggest that for a well-designed system whose true level of crosstalk is lower than $-20\,\mathrm{dB}$, reliable estimates can be obtained provided that the mean FRA at the calibration site is within $\pm 15^\circ$ and that the FRA can be suitably modeled as Gaussian. These sufficient conditions for successful application of DT-based algorithms have been validated via experiments on simulated data.

The calibration methods for both the normal and abnormal scenes were devised. For normal scenes, the equivalent system distortion matrix, $\boldsymbol{D}'$, can be readily obtained via direct application of DT-based algorithms. Experiments on simulated data suggested the propose method outperforms the Freeman's

method as long as the crosstalk level is above −50 dB. Calibration of the abnormal scenes can be straightforwardly achieved through correction of $\boldsymbol{D}'$ for a stable system. The residual FRA can be estimated and corrected using the circular-polarization-based method. However, for an unstable system, after correction of the DM, the distortions caused by amplifier drift still remain. This aspect will be investigated in the future work.

To assess the performance of DT-based calibration algorithms, we also established a new set of criteria in terms of the MNE in accordance with the CEOS recommendations. These criteria are directly related to the residual distortions in the calibrated data and are thus more suitable than the conventional relative error metric for assessing the performance of a DT-based calibration algorithm.

Acknowledgements This work was supported by State Key Program of National Natural Science of China (Grant No. 61430118).

Conflict of interest The authors declare that they have no conflict of interest.

References

1 Rignot E J, Zimmermann R, van Zyl J J. Spaceborne applications of P-band imaging radars for measuring forest biomass. IEEE Trans Geosci Remote Sens, 1995, 33: 1162–1169
2 Lopez-Sanchez J M, Hajnsek I, Ballester-Berman J D. First demonstration of agriculture height retrieval with PolInSAR airborne data. IEEE Geosci Remote Sens Lett, 2012, 9: 242–246
3 Guo S L, Li Y, Hong W, et al. Model-based target decomposition with the π/4 mode compact polarimetry data. Sci China Inf Sci, 2016, 59: 062307
4 Freeman A. Calibration of linearly polarized polarimetric SAR data subject to Faraday rotation. IEEE Trans Geosci Remote Sens, 2004, 42: 1617–1624
5 Touzi R, Shimada M. Polarimetric PALSAR calibration. IEEE Trans Geosci Remote Sens, 2009, 47: 3951–3959
6 Kimura H. Calibration of polarimetric PALSAR imagery affected by Faraday rotation using polarization orientation. IEEE Trans Geosci Remote Sens, 2009, 47: 3943–3950
7 Villa A, Iannini L, Giudici D, et al. Calibration of SAR polarimetric images by means of a covariance matching approach. IEEE Trans Geosci Remote Sens, 2015, 53: 674–686
8 van Zyl J J. Calibration of polarimetric radar images using only image parameters and trihedral corner reflector responses. IEEE Trans Geosci Remote Sens, 1990, 28: 337–348
9 Freeman A, van Zyl J J, Klein J D, et al. Calibration of stokes and scattering matrix format polarimetric SAR data. IEEE Trans Geosci Remote Sens, 1992, 30: 531–539
10 Klein J D. Calibration of complex polarimetric SAR imagery using backscatter correlations. IEEE Trans Aerosp Electron Syst, 1992, 28: 183–194
11 Touzi R, Livingstone C E, Lafontaine J R C, et al. Consideration of antenna gain and phase patterns for calibration of polarimetric SAR data. IEEE Trans Geosci Remote Sens, 1993, 31: 1132–1145
12 Quegan S. A unified algorithm for phase and cross-talk calibration of polarimetric data — theory and observations. IEEE Trans Geosci Remote Sens, 1994, 32: 89–99
13 Ainsworth T L, Ferro-Famil L, Lee Jong-Sen. Orientation angle preserving a posteriori polarimetric SAR calibration. IEEE Trans Geosci Remote Sens, 2006, 44: 994–1003
14 Goh A, Preiss M, Gray D, et al. Comparison of parameter estimation accuracy of distributed-target polarimetric calibration techniques. In: IEEE International Geoscience and Remote Sensing Symposium (IGARSS), Barcelona, 2007. 4175–4178
15 Zhang H, Lu W, Zhang B, et al. Improvement of polarimetric SAR calibration based on the Ainsworth algorithm for Chinese airborne PolSAR data. IEEE Geosci Remote Sens Lett, 2013, 10: 898–902
16 Meyer F J, Nicoll J B. Prediction, detection, and correction of Faraday rotation in full-polarimetric L-band SAR data. IEEE Trans Geosci Remote Sens, 2008, 46: 3076–3086
17 Gail W. A simplified calibration technique for polarimetric radars. In: Proceedings of IEEE International Geoscience and Remote Sensing Symposium (IGARSS), Tokyo, 1993. 2: 377–379
18 Freeman A, Saatchi S S. On the detection of Faraday rotation in linearly polarized L-band SAR backscatter signatures. IEEE Trans Geosci Remote Sens, 2004, 42: 1607–1616
19 Wright P A, Quegan S, Wheadon N S, et al. Faraday rotation effects on L-band spaceborne SAR data. IEEE Trans Geosci Remote Sens, 2003, 41: 2735–2744
20 Sandberg G, Eriksson L E B, Ulander L M H. Measurements of Faraday rotation using polarimetric PALSAR images. IEEE Geosci Remote Sens Lett, 2009, 6: 142–146
21 Wright P, Meadows P, Mack G, et al. Aden ALOS-PALSAR product verification. In: Proceedings of European Space Agency Special Publication (ESA SP), Rhodes, 2008. 664
22 Lavalle M, Solimini D, Pottier E, et al. Faraday rotation estimation from unfocussed raw data: analysis using ALOS-PALSAR data. In: Proceedings of European Space Agency Special Publication (ESA SP), Frascati, 2009. 668

23 Bickel S H, Bates R H T. Effects of magneto-ionic propagation on the polarization scattering matrix. Proc IEEE, 1965, 53: 1089–1091
24 Wang Y T, Ainsworth T L, Lee J-S. Assessment of system polarization quality for polarimetric SAR imagery and target decomposition. IEEE Trans Geosci Remote Sens, 2011, 49: 1755–1771

Appendix A Proof of (10)

First, we present three intermediate results that will be used in the derivation of the equivalent form of the ESM. The 1st intermediate equation is

$$\boldsymbol{X}\left(u,v,w,z\right)\boldsymbol{A}\left(\alpha\right)\boldsymbol{K}\left(k\right)=\boldsymbol{K}\left(k\right)\boldsymbol{A}\left(\alpha\right)\boldsymbol{X}\left(u_0,v_0,w_0,z_0\right), \tag{A1}$$

where $u_0=uk$, $v_0=v/k\alpha$, $w_0=w/k$, and $z_0=zk\alpha$. The 2nd is

$$\boldsymbol{X}\left(u_0,v_0,w_0,z_0\right)\boldsymbol{\Omega}(\overline{\omega})=Y_1\boldsymbol{K}\left(k_1\right)\boldsymbol{A}\left(\alpha_1\right)\boldsymbol{X}\left(u_1,v_1,w_1,z_1\right). \tag{A2}$$

The definitions of the variables on the RHS of (A2) are

$$\begin{gathered}Y_1=\frac{(1-z_0t)(1+u_0t)}{1+t^2},\quad k_1=\frac{1-w_0t}{1+u_0t},\quad \alpha_1=\frac{(1+v_0t)(1+u_0t)}{(1-z_0t)(1-w_0t)},\\ u_1=\frac{u_0-t}{1+u_0t},\quad v_1=\frac{v_0-t}{1+v_0t},\quad w_1=\frac{w_0+t}{1-w_0t},\quad z_1=\frac{z_0+t}{1-z_0t},\end{gathered} \tag{A3}$$

where $t=\tan\overline{\omega}$. The last intermediate equation is

$$\boldsymbol{K}\left(k'\right)\boldsymbol{A}\left(\alpha'\right)\boldsymbol{X}\left(u_1,v_1,w_1,z_1\right)=\boldsymbol{X}\left(u',v',w',z'\right)\boldsymbol{A}\left(\alpha'\right)\boldsymbol{K}\left(k'\right), \tag{A4}$$

where $u'=u_1/k'$, $v'=v_1k'\alpha'$, $w'=w_1k'$, and $z'=z_1/k'\alpha'$. Combining (A1), (A2), and (A4) yields the following:

$$\begin{aligned}&Y\boldsymbol{X}\left(u,v,w,z\right)\boldsymbol{A}(\alpha)\boldsymbol{K}(k)\boldsymbol{\Omega}\left(\overline{\omega}\right)\\ &=Y\boldsymbol{K}\left(k\right)\boldsymbol{A}\left(\alpha\right)\boldsymbol{X}\left(u_0,v_0,w_0,z_0\right)\boldsymbol{\Omega}\left(\overline{\omega}\right)\\ &=YY_1\boldsymbol{K}\left(k\right)\boldsymbol{A}\left(\alpha\right)\boldsymbol{K}\left(k_1\right)\boldsymbol{A}\left(\alpha_1\right)\boldsymbol{X}\left(u_1,v_1,w_1,z_1\right)\\ &=YY_1\boldsymbol{K}\left(kk_1\right)\boldsymbol{A}\left(\alpha\alpha_1\right)\boldsymbol{X}\left(u_1,v_1,w_1,z_1\right)\\ &=Y'\boldsymbol{K}\left(k'\right)\boldsymbol{A}\left(\alpha'\right)\boldsymbol{X}\left(u_1,v_1,w_1,z_1\right)\\ &=Y'\boldsymbol{X}\left(u',v',w',z'\right)\boldsymbol{A}\left(\alpha'\right)\boldsymbol{K}\left(k'\right),\end{aligned} \tag{A5}$$

where $Y'=YY_1$, $k'=kk_1$, $\alpha'=\alpha\alpha_1$, $u'=u_1/k'$, $v'=v_1k'\alpha'$, $w'=w_1k'$, and $z'=z_1/k'\alpha'$. With a bit more effort, these variables can be expressed as in (11). Note that the following properties of the matrices $\boldsymbol{A}(\alpha)$ and $\boldsymbol{K}(k)$ were used in the derivation of (A5):

$$\boldsymbol{A}(\alpha_1)\boldsymbol{A}(\alpha_2)=\boldsymbol{A}(\alpha_1\alpha_2), \tag{A6}$$

$$\boldsymbol{K}(k_1)\boldsymbol{K}(k_2)=\boldsymbol{K}(k_1k_2), \tag{A7}$$

$$\boldsymbol{A}(\alpha)\boldsymbol{K}(k)=\boldsymbol{K}(k)\boldsymbol{A}(\alpha). \tag{A8}$$

Appendix B Proof of (22)

First, we derive the value of $\max_{\boldsymbol{\theta}}\{|u'(\boldsymbol{\theta},\overline{\omega})|\}$. Substituting the expression for u' into this expression, we obtain

$$\max_{\boldsymbol{\theta}}\left\{\left|u'(\boldsymbol{\theta},\overline{\omega})\right|\right\}=\max_{\boldsymbol{\theta}}\left\{\frac{|u-t/k|}{|1-wt/k|}\right\}. \tag{B1}$$

Because we have assumed that $|\overline{\omega}|\leqslant 45^\circ$, $|wt/k|<1$. The denominator on the RHS of (B1) achieves its minimum value of $1-xf|t|$ when $|w|=x$, $|k|=f^{-1}$, and $\arg\{w\}+\arg\{-t/k\}=\pi$. The numerator on the RHS of (B1) achieves its maximum value of $x+f|t|$ when $|u|=x$, $|k|=f^{-1}$, and $\arg\{u\}=\arg\{-t/k\}$. Hence, when $|u|=x$, $|w|=x$, $|k|=f^{-1}$, and $\arg\{u\}=\arg\{-t/k\}=\pi-\arg\{w\}$, the RHS of (B1) is maximized, with a value of $(x+f|t|)/(1-xf|t|)$. Thus, we have

$$\max_{\boldsymbol{\theta}}\left\{\left|u'(\boldsymbol{\theta},\overline{\omega})\right|\right\}=\frac{x+f|t|}{1-xf|t|}. \tag{B2}$$

Using the same approach, we can show that the values $\max_{\boldsymbol{\theta}}\{|v'(\boldsymbol{\theta},\overline{\omega})|\}$, $\max_{\boldsymbol{\theta}}\{|w'(\boldsymbol{\theta},\overline{\omega})|\}$, and $\max_{\boldsymbol{\theta}}\{|z'(\boldsymbol{\theta},\overline{\omega})|\}$ are all equal to $(x+f|t|)/(1-xf|t|)$. Therefore, we have

$$\widetilde{x}'(\overline{\omega})=\max_{\boldsymbol{\theta}}\left\{x'(\boldsymbol{\theta},\overline{\omega})\right\}=\frac{x+f|t|}{1-xf|t|}. \tag{B3}$$

Appendix C Proof of (25)

Based on (1) the assumption of azimuthal symmetry and (2) the reciprocity principle, we have

$$\langle S_{\mathrm{HH}}S_{\mathrm{VH}}^*\rangle=\langle S_{\mathrm{HH}}S_{\mathrm{HV}}^*\rangle=\langle S_{\mathrm{VV}}S_{\mathrm{VH}}^*\rangle=\langle S_{\mathrm{VV}}S_{\mathrm{HV}}^*\rangle=0 \tag{C1}$$

and

$$\langle S_{\rm VH} S_{\rm VH}^* \rangle = \langle S_{\rm HV} S_{\rm HV}^* \rangle = \langle S_{\rm VH} S_{\rm HV}^* \rangle. \tag{C2}$$

These two assumptions are adopted to ensure that the true target covariance matrix satisfies

$$\boldsymbol{\Sigma} = \begin{bmatrix} \Sigma_{11} & 0 & 0 & \Sigma_{14} \\ 0 & \Sigma_{\times} & \Sigma_{\times} & 0 \\ 0 & \Sigma_{\times} & \Sigma_{\times} & 0 \\ \Sigma_{14}^* & 0 & 0 & \Sigma_{44} \end{bmatrix}, \tag{C3}$$

where $\Sigma_{11} \triangleq \langle |S_{\rm HH}|^2 \rangle$, $\Sigma_{44} \triangleq \langle |S_{\rm VV}|^2 \rangle$, $\Sigma_{\times} \triangleq \langle |S_{\rm VH}|^2 \rangle$, and $\Sigma_{14} \triangleq \langle S_{\rm HH} S_{\rm VV}^* \rangle$.

Under FR conditions, using the results presented above and adopting the assumption that the backscatter and $\Delta\omega$ (and, hence, functions of $\Delta\omega$) are independent, the matrix terms in $\boldsymbol{\Sigma}'$ can be evaluated to be

$$\Sigma'_{11} = +a_4 \Sigma_{11} - a_2 \Sigma_{14} - a_2 \Sigma_{14}^* + a_0 \Sigma_{44}, \tag{C4}$$

$$\Sigma'_{14} = -a_2 \Sigma_{11} + a_4 \Sigma_{14} + a_0 \Sigma_{14}^* - a_2 \Sigma_{44}, \tag{C5}$$

$$\Sigma'_{44} = +a_0 \Sigma_{11} - a_2 \Sigma_{14} - a_2 \Sigma_{14}^* + a_4 \Sigma_{44}, \tag{C6}$$

$$\Sigma'_{22} = \Sigma_{\times} + a_2 \left(\Sigma_{11} + \Sigma_{14} + \Sigma_{14}^* + \Sigma_{44} \right), \tag{C7}$$

$$\Sigma'_{23} = \Sigma_{\times} - a_2 \left(\Sigma_{11} + \Sigma_{14} + \Sigma_{14}^* + \Sigma_{44} \right), \tag{C8}$$

$$\Sigma'_{33} = \Sigma_{\times} + a_2 \left(\Sigma_{11} + \Sigma_{14} + \Sigma_{14}^* + \Sigma_{44} \right), \tag{C9}$$

$$\Sigma'_{21} = -a_3 \Sigma_{11} - a_3 \Sigma_{14}^* + a_1 \Sigma_{14} + a_1 \Sigma_{44}, \tag{C10}$$

$$\Sigma'_{31} = +a_3 \Sigma_{11} + a_3 \Sigma_{14}^* - a_1 \Sigma_{14} - a_1 \Sigma_{44}, \tag{C11}$$

$$\Sigma'_{24} = +a_1 \Sigma_{11} + a_1 \Sigma_{14}^* - a_3 \Sigma_{14} - a_3 \Sigma_{44}, \tag{C12}$$

$$\Sigma'_{34} = -a_1 \Sigma_{11} - a_1 \Sigma_{14}^* + a_3 \Sigma_{14} + a_3 \Sigma_{44}, \tag{C13}$$

where

$$a_n = \langle \cos^n \Delta\omega \, \sin^{4-n} \Delta\omega \rangle, \quad n = 0, 1, \ldots, 4. \tag{C14}$$

Because $\boldsymbol{\Sigma}'$ is Hermitian by construction, the other terms can be straightforwardly obtained. Note that the identity $a_4 + 2a_2 + a_0 = 1$ was used in the derivation of Σ'_{22}, Σ'_{23}, and Σ'_{33}.

Finally, if $\Delta\omega$ is symmetrically distributed about zero, then $a_1 = a_3 = 0$ and a_4, a_2, and a_0 are positive real numbers. As a result, we have

$$\Sigma'_{22} = \Sigma'_{33}, \tag{C15}$$

$$\mathrm{Im}\{\Sigma'_{22}\} = \mathrm{Im}\{\Sigma'_{33}\} = \mathrm{Im}\{\Sigma'_{23}\} = 0, \tag{C16}$$

$$\mathrm{Im}\{\Sigma'_{11}\} = \mathrm{Im}\{\Sigma'_{44}\} = 0, \tag{C17}$$

$$\Sigma'_{21} = \Sigma'_{31} = \Sigma'_{24} = \Sigma'_{34} = 0, \tag{C18}$$

and

$$\begin{aligned} \Sigma'_{22} - \Sigma'_{23} &= 2a_2 \left(\Sigma_{11} + \Sigma_{14} + \Sigma_{14}^* + \Sigma_{44} \right) = 2a_2 \langle |S_{\rm HH} + S_{\rm VV}|^2 \rangle \\ &\geqslant 0. \end{aligned} \tag{C19}$$

Thus, $\boldsymbol{\Sigma}'$ takes the desired form, as expressed in (25).

Specifically, if $\Delta\omega \sim \mathcal{N}(0, \sigma_{\omega}^2)$, then we can compute the values of the a_n as follows:

$$\begin{gathered} a_4 = \left(3 + \exp\{-8\sigma_{\omega}^2\} + 4 \exp\{-2\sigma_{\omega}^2\} \right) / 8 > 0, \\ a_2 = \left(1 - \exp\{-8\sigma_{\omega}^2\} \right) / 8 \geqslant 0, \\ a_0 = \left(3 + \exp\{-8\sigma_{\omega}^2\} - 4 \exp\{-2\sigma_{\omega}^2\} \right) / 8 \geqslant 0, \\ a_1 = a_3 = 0. \end{gathered}$$

Note that $a_2 = 0$ only if $\sigma_{\omega} = 0$, which represents the constant FR condition; thus, the equality in (C19) holds only in the case of constant FR.